Article

Journal of the Brazilian Chemical Society

https://dx.doi.org/10.21577/0103-5053.20240170

*J. Braz. Chem. Soc.* **2025**, *36*, 3, e-20240170, 1-11


# A Novel Nanocomposite Based on (*Zea mays*) Corn Cob Biochar and Maghemite for the Competitive Adsorption of Endocrine Disruptor Compounds

*Carolina S. Cardoso,[a] Mayara da Silva,[a] Rodrigo Henrique Saatkamp,[a] Natália B. Caon,[a] Giuliana Valentini,[a] Alexandre Luis Parize[a] and Luciano Vitali*[,a]*

[a]*Departamento de Química, Universidade Federal de Santa Catarina, 88035-972 Florianópolis-SC, Brazil*

Faced with the global challenge of water treatment, the investigation of the removal of endocrine disruptor compounds (EDCs) in aquatic environments is essential to protect human and animals health. In this study, a novel nanocomposite was prepared from biochar from agricultural waste (corn cob) and maghemite ($\gamma$-$Fe_2O_3$) nanoparticles, named $PCC_N$, to remove four EDCs (triclosan, 17$\alpha$-ethinylestradiol, methylparaben, and bisphenol A) from aqueous solutions by adsorption. For the characterization of $PCC_N$, the advanced techniques Fourier transform infrared spectroscopy (FTIR), Brunauer-Emmett-Teller analysis (BET), pH of point of zero charge ($pH_{pzc}$), scanning electron microscopy (SEM), transmission electron microscopy (TEM), X-ray diffraction (XRD) and thermogravimetry (TGA) were employed. Competitive adsorption equilibrium studies of EDCs were performed with $PCC_N$ and compared to unmodified biochar (PCC). The pH effect showed that optimal adsorption of EDCs was at pH 8.0 for PCC and pH 6.0 for $PCC_N$. The salt concentration did not influence EDCs in the adsorption. In the adsorption isotherm, the results fitted the Freundlich isotherm model ($R^2 > 0.903$) and the adsorption kinetics were well described by the pseudo-second-order model ($R^2 > 0.985$). Furthermore, the desorption studies indicated that the $PCC_N$ can be reused. Thus, the investigation suggests $PCC_N$ has promising potential in the removal of EDCs from wastewater.

**Keywords:** nanocomposite, endocrine disruptor compounds, biochar, competitive adsorption, wastewater treatment

## Introduction

The presence of endocrine disruptor compounds (EDCs) in untreated surface water can have harmful implications for human health and animals, as they can cause hormonal dysfunctions and diseases such as cancer.[1,2] EDCs belong to a broad category of emerging contaminants that include plasticizers, parabens, aromatic hydrocarbons, steroid hormones, and alkylphenols, which are common substances present in daily life.[3] Therefore, innovative approaches are needed to remove these compounds from water bodies, aiming to protect both people's health and water ecosystems. In this context, adsorption is a process with great potential for removing EDCs from wastewater. The adsorption technique can be applied due to its advantages, such as low cost, simplicity, high efficiency, and ease of use. Furthermore, a wide range of cheap and effective materials can be used as adsorbents, such as biochar, which has been increasingly used as an adsorbent for the removal of various pollutants.[4,5]

Biochar is a material known for its high carbonaceous content, and it can be produced by the pyrolysis of agricultural waste in the absence of oxygen.[6,7] This material has been the subject of growing global interest, especially due to its environmental benefits such as ease of production, low cost, large-scale applicability, and potential for reuse. Recent works have explored its applications in the removal of EDCs. For example, Ponnuchamy *et al.*[8] proposed a promising approach for removing bisphenol A from aqueous environments using biochar derived from agricultural waste, specifically sugarcane bagasse. The biochar production from agricultural waste is especially relevant in countries with wide access to lignocellulosic biomass, such as Brazil, which produced more than 100 million tons of corn (*Zea mays*) in 2023.[9] Besides representing a sustainable approach, the use of biochar adds value to materials that would previously have been discarded and enables the effective removal of contaminants. Biochar can also be modified after pyrolysis

*e-mail: luciano.vitali@ufsc.br
Editor handled this article: Izaura C. N. Diógenes

to increase EDC removal performance, for example, by incorporating nanoparticles into the surface.[4,10] Thus, combining the advantages of biochar with nanoparticles, for instance, can lead to the formation of nanocomposites. Nanocomposites can be produced by various methods, such as the co-precipitation of iron oxides in biochar, in which nanoparticles, such as maghemite ($\gamma$-$Fe_2O_3$), have aroused interest in various areas of technology, especially in the removal of contaminants from water.[11,12]

Nanocomposites are produced by mixing a matrix, which can be polymeric, with a nanomaterial.[13] Therefore, combining the availability of many functional groups in pyrolyzed biochar, such as hydroxyl (OH) and carboxyl groups, with the large area of a specific surface, inherent to the nanomaterial, can produce promising nanocomposites for the removal of EDCs. The versatility of nanocomposites is due to their ability to undergo functionalization, making the material a potential adsorbent for wastewater treatment.[7,14-18]

Current literature shows a gap in research into competitive adsorption of the EDCs by nanocomposites.[19] In this way, this study stands out for introducing a novel nanocomposite, resulting from a sustainable methodology that combines the properties of biochar from agricultural waste with maghemite ($\gamma$-$Fe_2O_3$) nanoparticles. Therefore, this study aimed to investigate the adsorption capacity of a novel nanocomposite based on pyrolyzed corn cob biochar and nanoparticles from maghemite ($PCC_N$). The adsorption capacity was investigated by competitive adsorption equilibrium studies of four EDCs (triclosan (TCS), 17$\alpha$-ethinylestradiol (EE2), methylparaben (MePa), and bisphenol A (BPA)) in water. Equilibrium studies included the evaluation of the effect of pH, salt concentration, adsorption kinetics, adsorption isotherm, and desorption. The adsorption studies of EDCs in $PCC_N$ were compared with unmodified biochar (PCC). Thus, the novelty of our study lies in the absence of reported studies on the synthesis of the nanocomposite from corn cob biochar and maghemite nanoparticles for the competitive removal of four EDCs from the aqueous medium.

## Experimental

### Materials and methods

Analytical grade reagents and solutions were prepared using ultrapure water (Milli-Q system, Millipore, Bedford, USA). Individual solutions of the ECDs (MePa (≥ 99.0%), BPA (≥99.6%), EE2 (≥ 99.8%), and TCS (≥ 99.7%)) with a concentration of 100 mg $L^{-1}$ were prepared using high-purity standards and were purchased from Sigma-Aldrich (São Paulo, SP, Brazil). Acetonitrile (≥ 99.8%), employed as the mobile phase in high-performance liquid chromatography (HPLC) was of analytical grade HPLC and sourced from Sigma-Aldrich (São Paulo, SP, Brazil). Additionally, ethanol (≥ 99.8%) and sodium chloride (≥ 99.0%) reagents were of high purity and were obtained from Synth (São Paulo, SP, Brazil).

### Preparation of biochar (PCC) and nanocomposite ($PCC_N$)

The dried maize corn cobs were supplied by producers from Frederico Westphalen, RS, Brazil. The cobs were ground and then submitted to purification with ultrapure water and ethanol. For the pyrolysis process, the corn cob powder was put into a muffle with a controlled heating rate of 20 ºC $min^{-1}$ until 500 ºC and held for 60 min at this temperature under a nitrogen ($N_2$) atmosphere. After cooling to room temperature, the material was sieved using a 42-mesh screen, resulting in the PCC. A portion of the PCC was reserved for the subsequent adsorption studies, carried out to compare the pure biochar with the nanocomposite prepared in this study. The nanocomposite was prepared following the methodology proposed by Gurav *et al.*:[7] 200 mg of maghemite (produced and characterized as described in Caon *et al.*[20]) were dispersed in 100 mL of water through ultrasonic irradiation, and subsequently 1000 mg of PCC were added. The mixture underwent continuous agitation for 4 h at room temperature and pressure conditions. Subsequently, the nanocomposite was filtered, followed by successive washes with ultrapure water and oven drying at 60 °C for 24 h.

### Characterization of PCC and $PCC_N$

The materials were characterized by employing a variety of techniques. Attenuated total reflection (ATR) Fourier transform infrared spectroscopy (FTIR) analysis was conducted using the PerkinElmer Spectrum Two FTIR (Massachusetts, United States). Thermogravimetric analysis (TGA) was performed utilizing the TGA-50 Shimadzu analyzer up to 600 ºC with a heating rate of 10 °C $min^{-1}$ under a nitrogen atmosphere flowing at 50 mL $min^{-1}$ (Kyoto, Japan). Surface area evaluation was carried out through nitrogen adsorption at 77 K, following the Brunauer, Emmett, Teller (BET) method, utilizing the Quantachrome 2200 Novae (Boynton Beach, United States). The point of zero charge ($pH_{pzc}$) was determined in accordance with the approach outlined by Sadaf and Bhatti,[21] using a ZetaPlus model potentiostat Brookhaven (Malvern, United Kingdom), with buffer solutions containing 20 mg of each adsorbent at room

temperature. Scanning electron microscopy (SEM) was employed to assess morphology at two magnifications (×500 and ×1000) using the JEOL JSM-6390LV microscope. Samples were mounted on metal stubs and coated with cathodically sputtered gold using the LEICA SCD 500 model (Tokyo, Japan). Transmission electron microscopy (TEM) analyses were conducted using the JEOL JEM-2100 TEM microscope at an accelerating voltage of 200 kV (Tokyo, Japan). X-ray diffraction analysis was performed using a Bruker D2 Phase diffractometer with detector Lynxeye (Karlsruhe, Germany).

### HPLC monitoring of the EDCs

The monitoring of the EDCs was performed using an Agilent Technologies 1200 Series HPLC system (Waldbronn, Germany) equipped with a Synergi 4µ Polar-RP 80A column (150 × 2.0 mm ID, 4 µm particle size; Phenomenex, USA). The injection volume used was 20 µL and the flow rate was 0.5 mL $min^{-1}$. The mobile phases used were ultrapure water (A) and acetonitrile (B), and the gradient program applied was: 0 min 70% A; 3-5 min 30% A, and 7.5-10 min 70% A. The column temperature was maintained at 30 °C and the detection wavelength was set at 232 nm. The chromatographic separation of the EDCs is shown in Figure S1 (Supplementary Information (SI) section).

### Adsorption experiments

Adsorption equilibrium studies were carried out, including pH, salt concentration, kinetics, isotherms, and desorption assays. In all tests, the concentrations of EDCs were determined by high performance liquid chromatography (HPLC). The parameters affecting the adsorption process of EDCs by PCC and $PCC_N$ were evaluated using the same experimental procedures. In addition, the experiments were conducted in duplicate, and the standard deviations were used to represent the errors.

### Effect of pH

To assess the pH effect, 20 mg of each adsorbent was added to 10 mL of different buffer solutions, with pH ranging from 5 to 10, and distilled water (pH 6.7) containing 5 mg $L^{-1}$ of an EDCs mixture. The solutions were agitated at 80 rpm for 24 h at 25 °C and then centrifuged. The response used to evaluate this effect was the geometric mean of the q (mg $g^{-1}$) of each EDC as a function of each pH in the study range.

### Salt concentration

To assay the effect of salt on the adsorption of EDCs, different weights of sodium chloride (NaCl) were added to the solutions containing 20 mg of each adsorbent in 10 mL of a buffer solution (at pH 8.0 for the PCC and at pH 6.0 for the $PCC_N$). The salt concentration varied from 0.0 to 1.0 mol $L^{-1}$ and the solution contained 5 mg $L^{-1}$ of EDCs. The mixture of EDCs was agitated at 80 rpm for 24 h at room temperature and subsequently centrifuged. The response used to evaluate this effect was the geometric mean of the q (mg $g^{-1}$) of each EDC as a function of the salt concentration.

### Adsorption kinetics assays

The kinetic assays of the adsorption of EDCs were carried out in jacketed glassware using 100 mg of adsorbent and 100 mL of a solution containing 5 mg $L^{-1}$ of a mixture of EDCs, with the pH previously selected in the study of the effect of pH. The solutions underwent stirring at 400 rpm and room temperature. Aliquots of 500 µL were removed at intervals from 0 to 120 min, the period for the system to reach equilibrium. Subsequently, the supernatant was transferred to a microtube and centrifuged at 14000 rpm to separate the particles of adsorbent remaining in the solution. The response used to evaluate the adsorption kinetics was the ratio between the EDC concentration at time t ($C_t$) and the initial concentration ($C_i$) as a function of time. The experimental data were treated using the intraparticle diffusion, pseudo-first-order, and pseudo-second-order kinetic models.

### Adsorption isotherms assays

The experiments of the adsorption isotherms of EDCs for the adsorbents were carried out employing 10 mL of solutions with varying concentrations (2.5-20 mg $L^{-1}$) of EDCs at optimum adsorption pH, containing 20 mg of each adsorbent. The system was submitted to continuous agitation until equilibrium was reached. Subsequently, aliquots of the solutions were transferred to microtubes and centrifuged at 14000 rpm. The response of the adsorption isotherm evaluated was the q (mg $g^{-1}$) of each EDC as a function of the EDC concentration at equilibrium $C_{eq}$, (mg $L^{-1}$). The experimental data were treated using the Langmuir and Freundlich isotherm models.

### Desorption assays

The desorption experiments were conducted using a solution containing 10 mL of an EDCs mixture with a concentration of 5 mg $L^{-1}$ and 20 mg of PCCN at room temperature. After the adsorption, the EDCs retained by the $PCC_N$ were transferred to tubes containing an ethanol

solution with a concentration of 70% v/v for desorption. The mixture was stirred for 2 h at 80 rpm and 25 °C, followed by aliquot collection. To evaluate the desorption, the ratio between the desorbed peak area and the adsorbed peak area was calculated and then multiplied by 100.

## Results and Discussion

### Characterization of biochar (PCC) and nanocomposite ($PCC_N$)

The PCC and $PCC_N$ characterization were performed to gather information about their physical, chemical, and morphological properties, aiming to understand what mechanisms may be involved in the adsorption of EDCs. This aids in assessing the effectiveness of the materials as adsorbents. Furthermore, the characterization of adsorbent materials is critical to determine the optimal conditions for their utilization, including factors such as pH, salt concentration, equilibrium time, and isotherm, all of which contribute to increase the adsorption capacity of the adsorbents.

The FTIR results revealed changes in the chemical structure of the PCC resulting from the pyrolysis treatment (Figure S2, SI section). The RCC (raw corn cob) spectrum exhibits a peak at 2928 $cm^{-1}$ referring to the C–H aliphatic groups. The broad peak at 3440 $cm^{-1}$ is attributed to O–H stretching, associated with the hydroxyl functional group, present in phenols, alcohols, and carboxylic acids.[22,23] However, the PCC spectrum did not show this band, indicating that the O–H groups were suppressed due to pyrolysis, making the material a carbonaceous skeleton. Another significant change caused by pyrolysis was concerning the C–O (1115 $cm^{-1}$) groups related to cellulose and hemicellulose, which were changed, making the aromatic structure dominant. Furthermore, the band at 1413 $cm^{-1}$, attributed to aromatic C=C stretching vibration, and at 810 $cm^{-1}$, attributed to out-of-plane aromatic C–H vibration, confirmed the aromatization of the lignocellulosic biomass.[7,24] Moreover, the presence of the lignin compound is indicated by the peak around 1582 $cm^{-1}$ in the PCC, corresponding to the aromatic ring.[25] Finally, the peak at 571 $cm^{-1}$ in the $PCC_N$ spectrum can be attributed to the Fe–O vibration.[26] These results are relevant because the FTIR spectra of the $PCC_N$ show the presence of iron nanoparticles on the surface of the PCC and the presence of lignin in the biomass structure. It is important to note that the lignin molecule has aromatic rings, as do the EDCs. Thus, the structural similarity between EDCs and lignin suggests the possibility of π-π stacking interactions between EDCs and adsorbents.

The thermogravimetric analysis (TGA) indicated the degradation of cellulose and hemicellulose after pyrolysis due to the high amount of residual mass of the PCC and $PCC_N$ samples compared to RCC (Figure S3, SI section). In the dTG (derived thermogravimetry) curve, two characteristic events of cellulose and hemicellulose degradation are observed at approximately 202 and 394 °C, respectively. However, in the PCC and $PCC_N$ heating curves, these peaks associated with cellulose and hemicellulose degradation are not observed. In the two investigated materials (PCC and $PCC_N$), only two distinct peaks of weight loss are verified, occurring around 500 °C, which suggests the possible degradation of lignin.[25] Both samples presented a weight loss event of 7.7, 9.4, and 10.1% respectively, at approximately 30 to 100 °C, referring to a possible loss of water or other solvents. The morphological features of RCC, PCC, and $PCC_N$, characterized by porous and rough surfaces, are presented in Figure 1. The surface underwent a pronounced increase in roughness after pyrolysis, displaying honeycomb-like configurations and heterogeneous openings, as seen in Figure 1b with 1000 times magnification. The presence of these pores may have acted as facilitators to nanoparticle immersion, leading to an increase in the surface area, as illustrated in Figure 1c. Consequently, the maghemite ($\gamma$-$Fe_2O_3$) particles likely started the nucleation process mainly within the confines of the porous network of the biochar, followed by a trajectory of progressive growth covering other locations throughout the surface of the material.

Figure 1 shows TEM images of PCC (Figure 1d), $PCC_N$ (Figure 1e) and maghemite (Figure 1f). Figure 1f shows pure maghemite, and by comparing this image with Figure 1e, it is possible to see the presence of maghemite nanoparticles in the $PCC_N$ structure. In Figure 1e, we see the cluster of maghemite nanoparticles contrasting with the carbon structures derived from biochar. Corroborating the previous statement, the XRD patterns for $PCC_N$, PCC and maghemite are shown in Figure S4 (SI section). The PCC diffractogram shows a first amorphous halo from 10 to 35 degrees and a second broad peak around 45 degrees that are characteristic of carbon materials, as expected for the biochar. Therefore, only amorphous phase is observed in the PCC sample. However, the XRD pattern of maghemite shows strong diffraction peaks at 18.3º, 30.2°, 35.5°, 43.2°, 53.6°, 57.1° and 62.7°, attributed to the (111), (220), (311), (400), (422), (511) and (440) crystal planes (ICSD card No. 172905).[20] The similar diffraction peaks are also observed in the $PCC_N$, although less intensely due to the small amount in wt.% of maghemite and diffraction contributions of amorphous biochar, confirming the presence of maghemite nanoparticles in the $PCC_N$ structure.

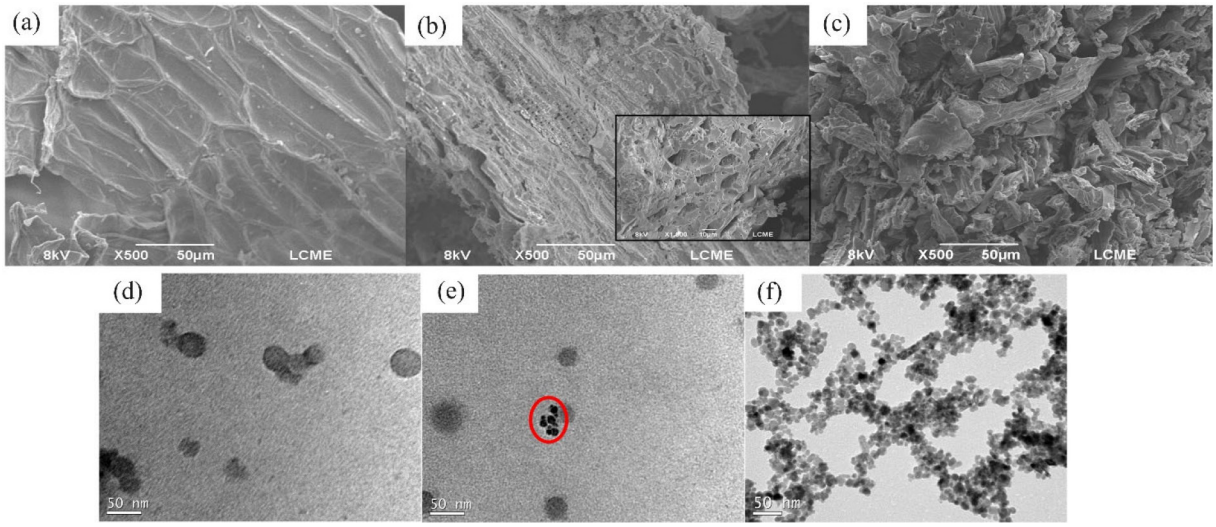


**Figure 1.** SEM images of the RCC (a), PCC (b), and $PCC_N$ (c). TEM images of the PCC (d), $PCC_N$ (e), and maghemite (f).

Therefore, it is evident that the novel nanocomposite of biochar with maghemite ($\gamma$-$Fe_2O_3$) nanoparticles is an adsorbent with high adsorption potential. This is due to the synergy of several factors, including the presence of available functional groups, the existence of pores capable of providing interaction between molecules and nanoparticles, and the increase in the surface area of the material. The enlargement of the surface area of the adsorbents is observed in the BET analysis in values of 7.00 and 19.03 $m^2\ g^{-1}$ for PCC and $PCC_N$, respectively. There was a significant change in the surface structure, since the available surface area of the $PCC_N$ increased by more than a 2-fold factor, as expected. Thus, RCC and PCC presented changes in their chemical structures when subjected to pyrolysis and by the superficial incorporation of maghemite, respectively, as evidenced by the results of the characterization analysis. Consequently, the changes observed from RCC to PCC and $PCC_N$ may contribute to better performance when interacting with EDCs.

## Adsorption studies

Adsorption equilibrium studies were conducted to assess the adsorption capacity of the materials. Investigating the pH effect, salt concentration, adsorption kinetics, adsorption isotherms, and desorption enhances the comprehension of the adsorbent's behavior concerning EDCs. This investigation also enables the determination of the optimal adsorption conditions for each adsorbent.

### Effect of pH

The influence of pH on adsorption was analyzed to identify the best adsorption pH. This parameter has a synergistic effect on adsorption capacity because it can cause the ionization of EDCs and the change in the surface charge of the adsorbent. To evaluate the adsorption equilibrium of the sorbents, we determined the adsorption capacity of each of them after 24 h. This study was established using q according to equation 1.

$$q = \frac{C_i - C_f}{m} \times V \quad (1)$$

where m (g) is the mass of the adsorbent, $C_i$ (mg $L^{-1}$) and $C_f$ (mg $L^{-1}$) are the initial and final concentrations, respectively, of EDCs in aqueous solution, and V (L) is the volume of the solution. Subsequently, the relationships of q *versus* pH for the adsorption of EDCs by adsorbents were plotted.

A compromise condition was adopted for an adequate selection of the adsorption pH of each adsorbent, due to the nature of competitive adsorption. This condition aimed to ensure that some EDCs were not prioritized for adsorption. In this sense, the geometric mean of q of all EDCs at each pH was considered for each adsorbent, as shown in Figure 2. According to the analysis of variance (ANOVA), the results were statistically different ($p < 0.05$) ($F_{cal} > F_{crit}$ for both adsorbents). Thus, the pH values selected for the adsorption process were 8.0 for PCC and 6.0 for $PCC_N$. It is important to highlight that the pH values chosen are aligned with the standards established by the Brazilian environmental standard CONAMA No. 430/2011,[27] which defines the conditions and standards of effluents discharge into a body of water. According to this standard, the pH must be in the range of 5.0 to 9.0.

To understand the effect of pH on the structure of adsorbents and EDCs, an analysis of the pH of zero charge potential ($pH_{pzc}$) was conducted to identify possible electrostatic interactions (Figure S5, SI section). The $pH_{pzc}$

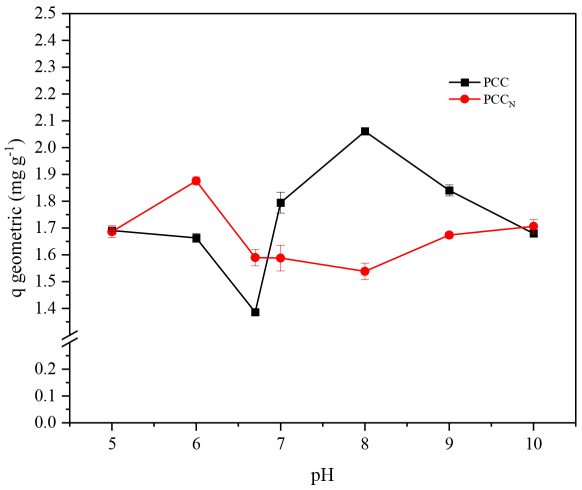


**Figure 2.** Compromise condition, geometric mean q (mg $g^{-1}$) of EDCs at each pH for PCC (-■-) (at pH 8.0) and $PCC_N$ (-●-) (at pH 6.0). Experimental conditions: 20 mg of adsorbent, 24 h of contact, stirring at 80 rpm and room temperature.

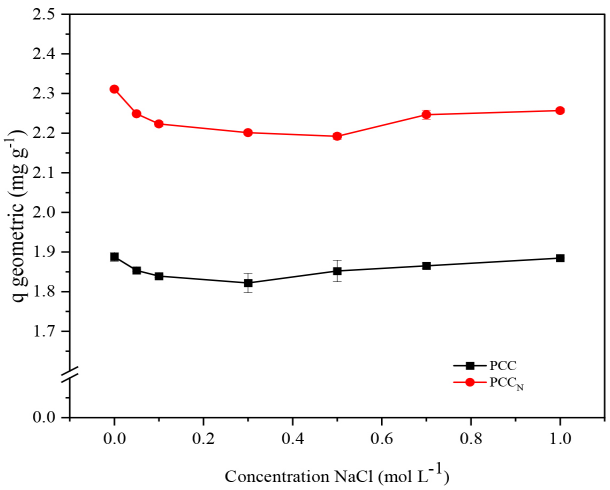


**Figure 3.** Compromise condition, geometric mean q (mg $g^{-1}$) of EDCs at each NaCl concentration (mol $L^{-1}$) for PCC (-■-) (at pH 8.0) and $PCC_N$ (-●-) (at pH 6.0). Experimental conditions: 20 mg of adsorbent, 24 h of contact, stirring at 80 rpm and room temperature.

determined for the PCC was 8.57, while for the $PCC_N$ it was 5.08. It is known that the surface of the adsorbent material acquires a positive charge when the solution pH is lower than the $pH_{pzc}$, and negative when the solution pH is higher than the $pH_{pzc}$.[21,28,29] For PCC, the solution pH was lower than $pH_{pzc}$, resulting in a positively charged surface. In contrast, for $PCC_N$, the solution pH was higher than $pH_{pzc}$, indicating a negatively charged adsorbent surface. However, when considering the p$K_a$ values of the EDCs (Table S3, SI section)[30-33] and the solution pH for each adsorbent, we can infer that there may have been a small electrostatic interaction between the EDCs MePa and TCS, which were negatively charged, with the positive surface of the PCC. On the other hand, for $PCC_N$, no electrostatic interactions were observed since EDCs at pH 6.0 are neutral.

### Salt concentration

The salt concentration on the adsorption process of EDCs on adsorbents was evaluated using sodium chloride (NaCl). The variation in the q as a function of NaCl concentrations in mol $L^{-1}$ was observed.

The geometric mean of q of EDCs as a function of the concentration of salt was adopted to select the most appropriate condition for the adsorption (Figure 3). According to ANOVA, the results were statistically different ($p < 0.05$) ($F_{cal} > F_{crit}$ for both adsorbents). The geometric mean profile indicated that the absence of salt presented better results in terms of q and, therefore, NaCl mass was not added to the next adsorption experiments for both adsorbents.

### Adsorption kinetics

The equilibrium time required for adsorption was determined for both adsorbents by analyzing the data of the adsorption kinetics of the EDCs. The experiments were conducted at the optimized pH for both systems: pH 8.0 for PCC and pH 6.0 for $PCC_N$. Graphs of q (mg $g^{-1}$) as a function of time (min) (Figure S6, SI section) were plotted and it was observed that the EDCs equilibrium was reached in less than 30 min for both adsorbents.

To elucidate the adsorption kinetic mechanism, the data were analyzed by applying pseudo-first-order, pseudo-second-order, and intraparticle diffusion kinetic models to observe the adsorption rate of molecules on the surface of an adsorbent (Table S1, SI section). These are the most common mathematical models used in liquid adsorption studies.[34,35] The experimental data on adsorption kinetics were adjusted to the previously mentioned kinetic models. The corresponding correlation coefficients are presented in Table 1.

The pseudo-second-order model proved to be the most suitable for fitting the data in all cases ($R^2 > 0.985$). This result agrees with the adsorption studies reported in the literature.[35] In this model, the saturation of the adsorbent surface occurs progressively. That is, as the surface of the adsorbents is saturated by EDCs, the adsorption rate decreases until it reaches an equilibrium state. Furthermore, this model also suggests that the adsorption is governed by a chemisorption mechanism, in which there are chemical interactions between the EDCs and the adsorbent and not a mass transfer in solution.[36] The analysis of the adsorption kinetic data using the pseudo-second-order kinetic model made it possible to determine the adsorption kinetic parameters, which are presented in Table 2.

The determined value of the equilibrium adsorption amount ($q_e$), derived from the pseudo-second-order

**Table 1.** Determination coefficients for the three kinetic models evaluated in the adsorption of MePa, BPA, EE2, and TCS by PCC and $PCC_N$

| EDC | Determination coefficient ($R^2$) | | | | | |
|---|---|---|---|---|---|---|
| | PCC | | | $PCC_N$ | | |
| | Pseudo-first-order[a] | Pseudo-second-order[b] | Intra-particle diffusion[c] | Pseudo-first-order[a] | Pseudo-second-order[b] | Intra-particle diffusion[c] |
| MePa | 0.591 | 0.998 | 0.641 | 0.504 | 0.998 | 0.912 |
| BPA | 0.705 | 0.999 | 0.818 | 0.307 | 0.999 | 0.562 |
| EE2 | 0.105 | 0.999 | 0.665 | 0.641 | 0.999 | 0.854 |
| TCS | 0.235 | 0.997 | 0.840 | 0.087 | 0.985 | 0.850 |

13 levels were used to construct the graphs of the MePa, BPA, EE2 and TCS kinetic models. [a]Kinetic model of pseudo-first-order; [b] kinetic model of pseudo-second-order; [c]kinetic model of intra-particle diffusion. EDC: endocrine disruptor compounds; MePa methylparaben; BPA: bisphenol A; EE2: 17α-ethinylestradiol; TCS: triclosan.

**Table 2.** Kinetic parameters and linear equations calculated from the pseudo-second-order model for the adsorption of MePa, BPA, EE2, and TCS by the PCC and $PCC_N$

| EDC | PCC | | | | $PCC_N$ | | | |
|---|---|---|---|---|---|---|---|---|
| | Linear equation | $k_2$[a] / (g $mg^{-1}$ $min^{-1}$) | $q_{e\ calc.}$[b] / (mg $g^{-1}$) | $q_{exp}$[b] / (mg $g^{-1}$) | Linear equation | $k_2$[a] / (g $mg^{-1}$ $min^{-1}$) | $q_{e\ calc.}$[b] / (mg $g^{-1}$) | $q_{exp}$[b] / (mg $g^{-1}$) |
| MePa | $y = 0.802x + 0.193$ | 3.327 | 1.246 | 1.268 | $y = 0.596x + 0.353$ | 1.00 | 1.673 | 1.574 |
| BPA | $y = 0.508x + 0.185$ | 1.395 | 1.968 | 1.966 | $y = 0.643x - 0.052$ | 7.907 | 1.553 | 1.591 |
| EE2 | $y = 0.383x + 0.142$ | 2.610 | 2.425 | 1.032 | $y = 0.399x + 0.134$ | 1.186 | 2.501 | 2.409 |
| TCS | $y = 0.894x + 0.318$ | 1.118 | 1.066 | 2.507 | $y = 2.211x + 2.431$ | 1.832 | 0.473 | 0.433 |

[a]The adsorption rate constant. [b]Amount adsorbed in the calculated equilibrium ($q_{e\ calc.}$) and experimental ($q_{exp}$). EDC: endocrine disruptor compounds; MePa: methylparaben; BPA: bisphenol A; EE2: 17α-ethinylestradiol; TCS: triclosan.

equation, can be compared with the experimentally determined value. The relative error between the values of $q_{e\ calc.}$ (calculated) and $q_{exp}$ (experimental) ranged from 1.73% in MePa adsorption to 4.84% in TCS adsorption by PCC, and from 2.37% for BPA to 9.36% in the adsorption of TCS by $PCC_N$. This confirmed that the experimental data accurately fits the pseudo-second-order kinetic equation.

The rate constants ($k_2$) are calculated using the pseudo-second-order model and represent the speed at which adsorption occurs. Considering the constants obtained, the order observed for PCC was MePa > EE2 > BPA > TCS. As for PCCN, the order was BPA > TCS > EE2 > MePa. A trend related to the log P of EDCs was observed in the results obtained in the $PCC_N$ study. Compounds with a log P value close to 3 showed a faster adsorption rate. MePa, which has a log P equal to 1.96, presented the lowest adsorption rate in this specific case (Table S3 contains the log P values of the EDCs).[30-33]

## Adsorption isotherm

The adsorption isotherm tests of EDCs by adsorbents were carried out using the adsorption pH previously selected in studies on the effect of pH (pH 8.0 for PCC and pH 6.0 for $PCC_N$) and the necessary contact time to achieve adsorption equilibrium. The isotherm is associated with the relationship between the adsorbate concentration in the solid phase and its equilibrium concentration in the aqueous phase. The application of isotherm models allows a theoretical analysis of the adsorption processes. We employed the Langmuir and Freundlich isotherm models (Table S2, SI section). The Langmuir isotherm represents a stage that highlights monolayer adsorption, where the adsorption sites have identical energies. In contrast, the Freundlich isotherm describes equilibrium on heterogeneous surfaces, such as amorphous surfaces, and, for this reason, does not assume a monolayer adsorption capacity.[37,38] The determination coefficients $R^2$ for the mentioned isotherm models are presented in Table 3.

**Table 3.** Determination coefficients for the isotherm models tested in the adsorption of MePa, BPA, EE2 and TCS by PCC and $PCC_N$

| EDC | Determination coefficient ($R^2$) | | | |
|---|---|---|---|---|
| | PCC | | $PCC_N$ | |
| | Langmuir[a] | Freundlich[b] | Langmuir[a] | Freundlich[b] |
| MePa | 0.415 | 0.993 | 0.744 | 0.994 |
| BPA | 0.185 | 0.989 | 0.960 | 0.997 |
| EE2 | 0.02 | 0.940 | 0.752 | 0.974 |
| TCS | 0.297 | 0.903 | 0.698 | 0.997 |

[a,b]8 levels were used to construct the graphs of the MePa, BPA, EE2 and TCS isotherm models. EDC: endocrine disruptor compounds; MePa methylparaben; BPA: bisphenol A; EE2: 17α-ethinylestradiol; TCS: triclosan.

When analyzing and comparing these values, the best fit for the experimental data was observed with the Freundlich isotherm. The Freundlich isotherm is often used to characterize adsorption on heterogeneous surfaces and to represent multilayer sorption processes with interactions between adsorbed molecules.[38] Therefore, we hypothesize that coating the PCC with maghemite nanoparticles has intensified the surface heterogeneity, which was already observed in the SEM images, and is corroborated by this isotherm. Currently, this isotherm is used in heterogeneous systems, such as organic compounds or chemical species that demonstrate affinity and interaction with activated carbon.[39] Based on the Freundlich equation, the values of Freundlich isothermal constant ($K_F$) and adsorption intensity (n) can establish the relationship between the slopes and intercepts of the linear fit curves, respectively. The constant $K_F$ represents the adsorption capacity, and the values of n represent the favorability of adsorption, where values greater than 1.0 indicate the favorable nature of the adsorption.[40] $K_F$ and the n values are presented in Table 4.

**Table 4.** Freundlich isotherm parameters for PCC and $PCC_N$

| EDC | PCC | | $PCC_N$ | |
|---|---|---|---|---|
| | n | $K_f$ / (mg $g^{-1}$) (mg $L^{-1}$)$^{1/n}$ | n | $K_f$ / (mg $g^{-1}$) (mg $L^{-1}$)$^{1/n}$ |
| MePa | 0.885 | 0.423 | 1.070 | 1.00 |
| BPA | 1.160 | 0.695 | 1.156 | 1.047 |
| EE2 | 1.248 | 0.887 | 1.165 | 1.117 |
| TCS | 0.880 | 0.394 | 0.877 | 0.605 |

n: adsorption intensity; $K_f$: Freundlich isothermal constant. EDC: endocrine disruptor compounds; MePa methylparaben; BPA: bisphenol A; EE2: 17α-ethinylestradiol; TCS: triclosan.

Based on the isotherm results, the coating and modification of the PCC with maghemite (γ-$Fe_2O_3$) nanoparticles, which resulted in the $PCC_N$, played an important role in increasing the adsorption capacity of the EDCs. It led to higher values of the Freundlich constant ($K_F$) in relation to the chemically unmodified PCC adsorbent. The order of magnitude of the $K_F$ values for the $PCC_N$ adsorbent was as follows: EE2 (1.11) > BPA (1.04) > MePa (1.00) > TCS (0.605) (mg $g^{-1}$) (mg $L^{-1}$)$^{1/n}$. However, when we evaluated the n values obtained for both adsorbents, we observed that they approached 1. This suggests, in general, that the adsorptions were favorable, due to the competitive nature of the isotherm between the EDCs.

According to the findings reported by Farias *et al.*,[41] the isotherms presented in Figure 4 do not exhibit a saturation trend, as higher quantities of $q_e$ were observed with increasing $C_e$. This underscores that adsorption extends beyond a monolayer to encompass multilayers, consistent with the predictions from the Freundlich model. Additionally, as depicted in Figure 4, at the highest concentration point investigated (20 mg $L^{-1}$), the amount adsorbed of each EDC was 18.74, 15.52, 13.54, and 13.08 mg $g^{-1}$ for TCS, MePa, EE2, and BPA, respectively. It amounts to a total of approximately 60 mg $g^{-1}$ of the four EDCs adsorbed on the $PCC_N$. Hence, $PCC_N$ demonstrates the capability to adsorb a mixture of EDCs onto its surface.

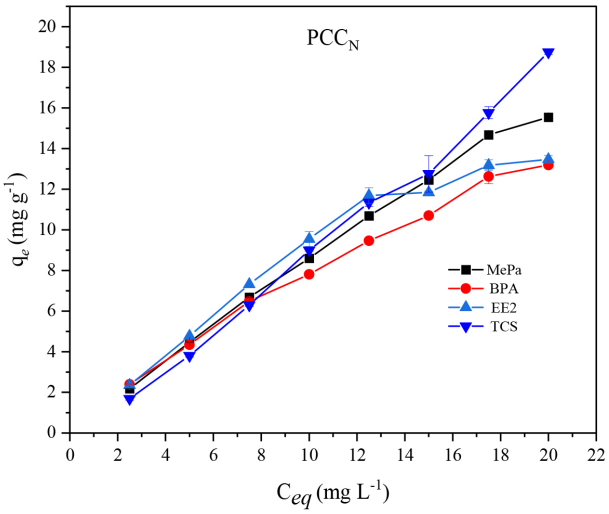


**Figure 4.** Adsorbed amount at equilibrium $q_e$ (mg $g^{-1}$) as a function of equilibrium concentration $C_{eq}$ (mg $L^{-1}$). MePa (-■-), BPA (-●-), EE2 (-▲-), and TCS (-▼-), at pH 6.0 for a $PCC_N$. Experimental conditions: 20 mg of adsorbent, 1 h of contact, agitation at 80 rpm and 25 °C.

## Desorption assays

Desorption analysis is an important parameter in adsorption processes, as it makes it possible to evaluate the reuse capacity of the adsorbent and reveals its potential in pre-concentration systems to apply the material as an extraction phase in sample preparation techniques, for example. In this context, ethanol stood out as a desorbing agent, being subjected to test at 70% v/v concentration for $PCC_N$, for 2 h. Desorption percentages were calculated with equation 2.

$$\text{Desorption efficiency (\%)} = \frac{\text{Desorbed Area}}{\text{Adsorption area}} \times 100 \quad (2)$$

The results of the desorption percentages obtained for EDCs are shown in Figure 5.

The percentage of desorption of EDCs from $PCC_N$ was greater than 65% using 70% v/v ethanol. This concentration proved to be effective in removing EDCs, allowing for at least one cycle of reuse. This indicates that ethanol is a suitable solvent for this purpose. Furthermore, it is worth noting that ethanol is classified as a green organic

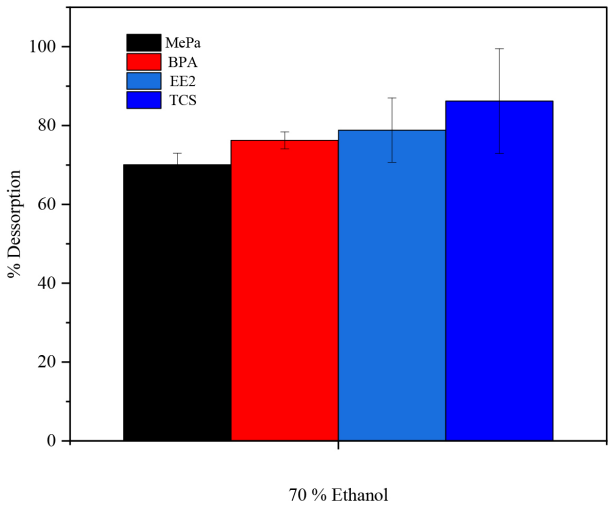


**Figure 5.** Percentage of desorption of EDCs from $PCC_N$ using ethanol at a concentration of 70% v/v after 2 h of desorption.

solvent, aligning with the principles of Green Chemistry, and making the nanocomposite production process more environmentally friendly.

## Comparison with other adsorbents

Table 5 summarizes some materials for the removal of endocrine compounds under different experimental conditions. When comparing the results of this study with other studies, it becomes apparent that the optimal pH for adsorption in most studies is higher than 5.

Additionally, the prevailing kinetic mechanism describing adsorption processes is typically pseudo-second-order, while the Langmuir or Freundlich isotherm models are frequently utilized. Few studies explore the reutilization and the impact of salt addition on adsorption, which are crucial aspects of the adsorption process. Reuse is important to make the process more environmentally friendly. Salt addition helps to understand the effect of salt on adsorption at different NaCl concentrations, since ions can influence the interactions between the adsorbent and the contaminants.

Several studies[8,28,41,42,45] address the removal of EDCs from aquatic ecosystems via adsorption. However, the lack

**Table 5.** Comparative summary of studies on the adsorption of EDCs by other adsorbents

| Adsorbent | EDC | pH | Salt concentration (NaCl) / (g $L^{-1}$) | Dosage | Kinetic model | Isothermal model | Amount adsorbed / (mg $g^{-1}$) | Reuse | Reference |
|---|---|---|---|---|---|---|---|---|---|
| Sugarcane bagasse derived biochar | bisphenol A | 6.0 | – | 20 mg | PSO[a] | Freundlich | 32.05 | – | 8 |
| Attapulgite/biochar nanocomposite | 17β-estradiol | 3.5 | 0.05 | 5 mg | PSO[a] | Langmuir | 154.32 | reusable | 42 |
| Spectrogel® (organoclay) | bisphenol A | pH neutral | – | 64 mg | external mass transfer resistance | Freundlich[b] | 55.77 | reusable | 41 |
| Magnetic porous organic cage adsorbent | bisphenols parabens hormones | independent of pH | – | 13 mg | PSO[a] | Langmuir | 29.66[c] | reusable | 43 |
| Fc-rGO/nZVI nanocomposite | bisphenol A | 12 | – | 200 mg $L^{-1}$ | PFO[d] | Langmuir | 16.35 | reusable | 44 |
| Double ionic liquid reinforced g-CN nanocomposite | methylparaben | pH neutral | – | 75 mg | PSO[a] | Freundlich | 267.2 | reusable | 45 |
| Activated carbon[e] | triclosan | 7.0 | – | 1 mg | diffusional | Prausnitz-Radke | 18.5 | – | 46 |
| Algae-based red mud catalyst activated persulfate | 17α-ethinylestradiol | 8.0 | – | 100 mg | PSO[a] | Langmuir | 8.0 | reusable | 47 |
| Single-walled carbon nanotubes | triclosan | 7.0 | – | – | PFO[d] | Prausnitz-Radke | 30.30 | – | 48 |
| $PCC_N$ | triclosan17α-ethinylestradiol methylparaben bisphenol A | 6.0 | independent of concentration | 20 mg | PSO[a] | Freundlich | 60.0 | reusable | this work |

[a]Pseudo-second-order (PSO). [b]In this work, the Freundlich isotherm model best described the data obtained at 15 and 25 °C, and Dubinin-Radushkevich was the best fit for those obtained at 40 and 55 °C. The maximum amount adsorbed shown in the table was at 25 °C. [c]This value is the combined adsorption capacity of two contaminants selected for isotherm evaluation: butylparaben at 16.15 mg $g^{-1}$ and bisphenol B at 13.51 mg $g^{-1}$. [d]Pseudo-first-order (PFO). [e]This study investigated the application of adsorption with activated carbons. The presented result refers to 'Darco' type activated carbon.

of research on competitive adsorption becomes apparent. The majority of studies concentrate on the adsorption of a singular EDC. Investigating competitive adsorption is pivotal for comprehending the behavior of the adsorbent in the presence of other contaminants.

Finally, the proposed nanocomposite shows great promise in effectively removing EDCs from aquatic environments. In comparison to other studies, this investigation revealed a significant outcome in terms of the amount of EDCs adsorbed, totaling approximately 60 mg $g^{-1}$. This result holds significance considering the competitive nature of adsorption, where competition arises between EDCs for interaction sites on the adsorbent.

## Conclusions

The results of this study described a novel nanocomposite and its characterization, revealing changes in the structure after the inclusion of maghemite nanoparticles. FTIR analysis confirmed the development of the carbonaceous structure, and TGA highlighted the presence of lignin. The SEM analysis showed pores in the material, facilitating the immersion of the nanoparticles, and increasing the surface area, thus enhancing the adsorption capacity. The pseudo-second-order model fitted the kinetic data well, just as the Freundlich isotherm also fitted the isotherm data, which revealed a multilayer adsorption phenomenon. The desorption studies indicated that the material can be reused. Finally, the novel nanocomposite showed prospects for applications for the removal of EDCs in wastewater treatment and as an extraction phase in sample preparation techniques.

## Supplementary Information

Supplementary data are available free of charge at http://jbcs.sbq.org.br as PDF file.

## Acknowledgments

The authors are thankful to the Conselho Nacional de Desenvolvimento Científico e Tecnológico (CNPq), Coordenação de Aperfeiçoamento de Pessoal de Nível Superior (CAPES - Financial Code 001) and INCT Catálise/FAPESC/CNPq/CAPES (FAPESC-2019TR0847, CNPq 444061/2018, A. L. P. process 305112/2022-8). We would like to thank Fabricio Faita, whose expertise enriched our analysis and interpretation of the XRD data. We are also grateful to Farma Service Bioextract for support.

### Author Contributions

Carolina S. Cardoso was responsible for the conceptualization, investigation, methodology, data curation, formal analysis, and writing original draft; Mayara da Silva for the methodology, formal analysis, writing-review and editing; Rodrigo Henrique Saatkamp for the methodology, formal analysis, writing-review and editing; Natália B. Caon for the methodology, formal analysis, writing-review and editing; Giuliana Valentini for the methodology, formal analysis, writing-review and editing; Alexandre Luis Parize for the supervision, writing-review and editing; Luciano Vitali for the conceptualization, writing-review and editing, project administration, and funding acquisition.

## References

1. Li, Y.; Reivan Ortiz, G. G.; Uyen, P. T. M.; Cong, P. T.; Othman, S. I.; Allam, A. A.; Unar, A.; Afridi, H. I.; *Environ. Res.* **2023**, *231*, 115913. [Crossref]
2. Chen, Y.; Yang, J.; Yao, B.; Zhi, D.; Luo, L.; Zhou, Y.; *Environ. Pollut.* **2022**, *310*, 119918. [Crossref]
3. Ismanto, A.; Hadibarata, T.; Kristanti, R. A.; Maslukah, L.; Safinatunnajah, N.; Kusumastuti, W.; *Environ. Pollut.* **2022**, *302*, 119061. [Crossref]
4. Zhang, J.; Chen, Z.; Liu, Y.; Wei, W.; Ni, B. J.; *Chem. Eng. J.* **2024**, *479*, 147615. [Crossref]
5. Rathi, B. S.; Kumar, P. S.; *Environ. Pollut.* **2021**, *280*, 116995. [Crossref]
6. Amusat, S. O.; Kebede, T. G.; Dube, S.; Nindi, M. M.; *J. Water Process Eng.* **2021**, *41*, 101993. [Crossref]
7. Gurav, R.; Bhatia, S. K.; Choi, T. R.; Park, Y. L.; Park, J. Y.; Han, Y. H.; Vyavahare, G.; Jadhav, J.; Song, H. S.; Yang, P.; Yoon, J. J.; Bhatnagar, A.; Choi, Y. K.; Yang, Y. H.; *Bioresour. Technol.* **2020**, *297*, 122472. [Crossref]
8. Ponnuchamy, M.; Kapoor, A.; Jacob, M. M.; Awasthi, A.; Mukhopadhyay, M.; Nandagobu, S.; Raghav, A.; Arvind, D.; Chakraborty, P.; Prabhakar, S.; *J. Taiwan Inst. Chem. Eng.* **2023**, 105216. [Crossref]
9. Instituto Brasileiro de Geografia e Estatística (IBGE), Levantamento Sistemático da Produção Agrícola, https://www.ibge.gov.br/estatisticas/economicas/agricultura-e-pecuaria/9201-levantamento-sistematico-da-producao-agricola.html?edicao=37367&t=resultados, accessed in August 2024.
10. Rajput, P.; Kumar, P.; Priya, A. K.; Kumari, S.; Shiade, S. R. G.; Rajput, V. D.; Fathi, A.; Pradhan, A.; Sarfraz, R.; Sushkova, S.; Mandzhieva, S.; Minkina, T.; Soldatov, A.; Wong, M. H.; Rensing, C.; *Sci. Total Environ.* **2024**, *916*, 170064. [Crossref]
11. Tan, X.-f.; Liu, Y.-g.; Gu, Y.-l.; Xu, Y.; Zeng, G.-m.; Hu, X.-J.; Liu, S.-b.; Wang, X.; Liu, S.-m.; Li, J.; *Bioresour. Technol.* **2016**, *212*, 318. [Crossref]

12. Asuha, S.; Gao, Y. W.; Deligeer, W.; Yu, M.; Suyala, B.; Zhao, S.; *J. Porous Mater.* **2011**, *18*, 581. [Crossref]
13. Namasivayam, S. K. R.; Prakash, P.; Babu, V.; Paul, E. J.; Bharani, R. S. A.; Kumar, J. A.; Kavisri, M.; Moovendhan, M.; *J. Cleaner Prod.* **2023**, *396*, 136386. [Crossref]
14. Rodriguez-Narvaez, O. M.; Peralta-Hernandez, J. M.; Goonetilleke, A.; Bandala, E. R.; *J. Ind. Eng. Chem.* **2019**, *78*, 21. [Crossref]
15. Han, H.; Rafiq, M. K.; Zhou, T.; Xu, R.; Mašek, O.; Li, X.; *J. Hazard. Mater.* **2019**, *369*, 780. [Crossref]
16. Liu, T.; Gao, B.; Fang, J.; Wang, B.; Cao, X.; *RSC Adv.* **2016**, *6*, 24314. [Crossref]
17. Inyang, M. I.; Gao, B.; Yao, Y.; Xue, Y.; Zimmerman, A.; Mosa, A.; Pullammanappallil, P.; Ok, Y. S.; Cao, X.; *Crit. Rev. Environ. Sci. Technol.* **2016**, *46*, 406. [Crossref]
18. Tan, X.; Liu, Y.; Zeng, G.; Wang, X.; Hu, X.; Gu, Y.; Yang, Z.; *Chemosphere* **2015**, *125*, 70. [Crossref]
19. Dong, M.; He, L.; Jiang, M.; Zhu, Y.; Wang, J.; Gustave, W.; Wang, S.; Deng, Y.; Zhang, X.; Wang, Z.; *Int. J. Environ. Res. Public Health* **2023**, *20*, 1679. [Crossref]
20. Caon, N. B.; Cardoso, C. D. S.; Faita, F. L.; Vitali, L.; Parize, A. L.; *J. Environ. Chem. Eng.* **2020**, *8*, 104003. [Crossref]
21. Sadaf, S.; Bhatti, H. N.; *J. Taiwan Inst. Chem. Eng.* **2014**, *45*, 541. [Crossref]
22. Ma, H.; Li, J. B.; Liu, W. W.; Miao, M.; Cheng, B. J.; Zhu, S. W.; *Bioresour. Technol.* **2015**, *190*, 13. [Crossref]
23. Vafakhah, S.; Bahrololoom, M. E.; Bazarganlari, R.; Saeedikhani, M.; *J. Environ. Chem. Eng.* **2014**, *2*, 356. [Crossref]
24. Fang, Q.; Chen, B.; Lin, Y.; Guan, Y.; *Environ. Sci. Technol.* **2014**, *48*, 279. [Crossref]
25. Padilla, E. R. D.; Nakashima, G. T.; Hansted, A. L. S.; Santos, L. R. O.; de Barros, J. L.; de Conti, A. C.; Yamaji, F. M.; *Quim. Nova* **2019**, *42*, 566. [Crossref]
26. Zhu, S.; Wang, S.; Yang, X.; Tufail, S.; Chen, C.; Wang, X.; Shang, J.; *J. Cleaner Prod.* **2020**, *276*, 123009. [Crossref]
27. Conselho Nacional do Meio Ambiente (CONAMA); Resolução No. 430/2011, *Dispõe sobre as Condições e Padrões de Lançamento de Efluentes, Complementa e Altera a Resolução No. 357, de 17 de março de 2005, do Conselho Nacional do Meio Ambiente-CONAMA*; Diário Oficial da União (DOU), Brasília, No. 92, de 16/05/2011, p. 89. [Link] accessed in August 2024
28. dos Santos Cardoso, C.; Vitali, L.; *Water, Air, Soil Pollut.* **2021**, *232*, 179. [Crossref]
29. Abdel Maksoud, M. I. A.; Elgarahy, A. M.; Farrell, C.; Al-Muhtaseb, A. H.; Rooney, D. W.; Osman, A. I.; *Coord. Chem. Rev.* **2020**, *403*, 213096. [Crossref]
30. PubChem, 17-alpha-Ethinylestradiol|$C_{20}H_{24}O_2$|CID 57495718, https://pubchem.ncbi.nlm.nih.gov/compound/5991, accessed in August 2024.
31. PubChem, Bisphenol A | $C_{15}H_{16}O_2$ | CID 6623, https://pubchem.ncbi.nlm.nih.gov/compound/6623, accessed in August 2024.
32. PubChem, Triclosan | $C_{12}H_7Cl_3O_2$ | CID 5564, https://pubchem.ncbi.nlm.nih.gov/compound/5564, accessed in August 2024.
33. PubChem, Methylparaben | $C_8H_8O_3$ | CID 7456, https://pubchem.ncbi.nlm.nih.gov/compound/7456, accessed in August 2024.
34. Abumelha, H. M.; Alzahrani, S. O.; Alrefaee, S. H.; Al-bonayan, A. M.; Alkhatib, F.; Saad, F. A.; El-Metwaly, N. M.; *J. Saudi Chem. Soc.* **2023**, *27*, 101706. [Crossref]
35. Tan, K. L.; Hameed, B. H.; *J. Taiwan Inst. Chem. Eng.* **2017**, *74*, 25. [Crossref]
36. Ho, Y. S.; Mckay, G.; *Process Biochem.* **1999** *34*, 451. [Crossref]
37. Langmuir, I.; *J. Am. Chem. Soc.* **1918**, *40*, 1361. [Crossref]
38. Freundlich, H. M. F.; *J. Phys. Chem.* **1906**, *57*, 385. [Crossref]
39. Foo, K. Y.; Hameed, B. H.; *Chem. Eng. J.* **2010**, *156*, 2. [Crossref]
40. Wang, M.; Wen, B.; Fan, B.; Zhang, H.; *Colloids Surf., A* **2020**, *599*, 124887. [Crossref]
41. de Farias, M. B.; Silva, M. G. C.; Vieira, M. G. A.; *Powder Technol.* **2022**, *395*, 695. [Crossref]
42. Yin, Z.; Liu, Y.; Tan, X.; Jiang, L.; Zeng, G.; Liu, S.; Tian, S.; Liu, S.; Liu, N.; Li, M.; *Process Saf. Environ. Prot.* **2019**, *121*, 155. [Crossref]
43. Xu, Q.; Zhang, W.; Chi, Q.; Yang, Y.; Tan, X.; Liu, J.; Xiao, H.; Wang, X.; *Chem. Eng. Sci.* **2024**, *285*, 119621. [Crossref]
44. Roy, N.; Sinha, A.; Mukherjee, A.; *Surf. Interfaces* **2024**, *44*, 103708. [Crossref]
45. Gholami, Z.; Foroughi, M.; Ahmadi Azqhandi, M. H.; *Chemosphere* **2024**, *349*, 141006. [Crossref]
46. Medellín-Castillo, N. A.; González-Fernández, L. A.; Ocampo-Pérez, R.; Leyva-Ramos, R.; Luiz-Dotto, G.; Flores-Ramírez, R.; Navarro-Frómeta, A. E.; Aguilera-Flores, M. M.; Carrasco-Marín, F.; Hernández-Mendoza, H.; Aguirre-Contreras, S.; Sánchez-Polo, M.; Ocaña-Peinado, F. M.; *Environ. Res.* **2024**, *246*, 118162. [Crossref]
47. He, H.; Yang, S.; Guo, Z.; Lai, C.; Yang, G.; Li, Z.; Xi, Y.; Wang, B.; Huang, B.; Pan, X.; *Sep. Purif. Technol.* **2024**, *342*, 126978. [Crossref]
48. González-Fernández, L. A.; Medellín-Castillo, N. A.; Ocampo-Pérez, R.; Hernández-Mendoza, H.; Berber-Mendoza, M. S.; Aldama-Aguilera, C.; *J. Environ Chem Eng.* **2021**, *9*, 106382. [Crossref]

*Submitted: April 25, 2024*
*Published online: August 21, 2024*